Investigations of Phononic Bandgap in a 3D Quantum-Dot Crystal

Yu-Chieh Wen,[1,2,*] Jia-Hong Sun,[3] Tsung-Tsong Wu,[3]
Christian Dais,[4] Detlev Grützmacher,[4,5] and Chi-Kuang Sun[1,2]

[1]*Department of Electrical Engineering and Institute of Photonics and Optoelectronics, National Taiwan University, Taipei 10617, Taiwan*
[2]*Institute of Physics, Academia Sinica, Taipei 115, Taiwan*
[3]*Institute of Applied Mechanics, National Taiwan University, Taipei 10617, Taiwan*
[4]*Laboratory for Micro- and Nanotechnology, Paul Scherrer Institut, 5232 Villigen, Switzerland*
[5]*Institute of Bio- and Nanosystems, Forschungszentrum Jülich, 52425 Jülich, Germany*

(Received April 12, 2010)

We theoretically study the phononic band-gap effect of an artificial nanocrystal composed of three-dimensionally (3D) ordered quantum dots. The calculated phonon dispersion indicates the existence of high-order longitudinal acoustic modes propagating along the growth direction due to the low aspect ratio of the unit cell. The observed phononic band gaps in the sub-THz frequency range result in high acoustic reflectivity of the nanocrystal at the band-gap frequencies. In addition to the phononic band gaps, the acoustic transmission spectrum reveals remarkable scattering loss at several specific frequencies, which could suggest the coupling between the longitudinal acoustic phonons and confined modes of isolated quantum dots. Our investigation provides a theoretical insight into the lattice dynamics of the quantum-dot crystal, complementary to the recent femtosecond ultrasonic experiment [*Appl. Phys. Lett.*, **96**, 123113 (2010)].

PACS numbers: 63.20.-e, 43.40.+s, and 63.22.-m

I. INTRODUCTION

Semiconductor quantum dots (QDs) are sometimes called artificial atom due to their unique characteristics for zero-dimensional charge confinement. With a controlled QD distribution, those "atoms" can create artificial materials with designed functionalities for electronic and biological applications [1]. In addition, the behaviors of phonons in a QD system are also dominated by the QD orderings. The understanding of lattice dynamics in 3D ordered QD systems is thus important for the control of electron-phonon and phonon-polariton interactions [2].

In the past decade, the dynamics of coherent acoustic phonons in QDs has attracted a lot of attention. Several literatures reported the observation of confined acoustic mode in QDs and also studied the exciton-coherent phonon interactions by femtosecond pump-probe technique [3]. A recent report by A. Devos *et al.* demonstrated an efficient generation of coherent acoustic phonons in self-assembled QD layers by laser excitation [4]. Those contributions revealed not only fundamental interests in this issue but also the potential of QD-based materials in phonon engineering [5]. However, the present studies on coherent

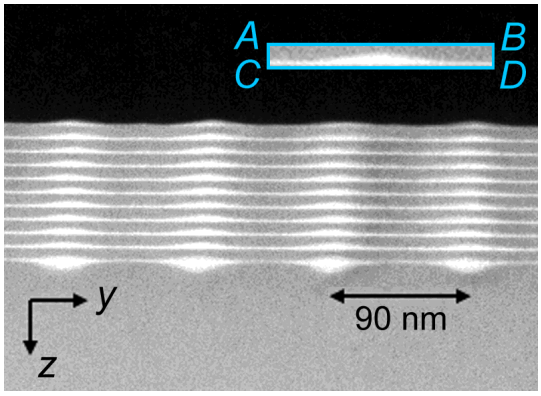

FIG. 1: TEM imaging of the studied QD crystal without the Si cap layer. The inset shows a unit cell of this nanocrystal.

phonons were restricted to either confined mode in QDs or collected propagating mode from a single QD layer. The structural effect on the coherent phonon dynamics in 3D regularized QDs is still far from understood. In this regard, noticeable efforts by (resonant) Raman spectroscopy and measurement of thermal transport have led to an insight into phonon propagations in ordered and disordered QD structures [6].

Very recently, we demonstrated the significant effects of the QD ordering and uniformity on the acoustic resonance at the forbidden bands using the femtosecond ultrasonic technique [7]. Here, we report a complementary theoretical study on the lattice dynamics in the same crystal by performing finite-difference time-domain (FDTD) calculations. Except the phononic band-gap frequencies, the calculated acoustic transmission spectrum reveals remarkable scattering loss at several specific frequencies, which could suggest that the energy of the longitudinal acoustic waves was transduced into vibrations of isolated quantum dots.

II. SAMPLE STRUCTURE

The studied sample is a 3D ordered SiGe QDs (QD crystal [2]) grown by templated self-organization. The templates were fabricated by extreme ultraviolet interference lithography using a wavelength of 13.5 nm. Reactive ion etching was employed to transfer the two-dimensional hole arrays with a periodicity of 90 nm $\times$ 100 nm into a Si(001) substrate. This prepatterned substrate was then deposited by a sequence of Ge and Si layers for fabricating a stack of 11 QD layers. It was noted that the growth condition of the first QD layer (7 ML) on the substrate was different from the other layers, resulting in a relatively large dot size in the first layer. Each subsequent island layer was grown by depositing 5 ML of Ge on top of the 10 nm Si spacer layer. Figure 1 shows a transmission electron microscope (TEM) image of the studied QD crystal. The TEM and X-ray analyses confirmed the periodicities and the 60% Ge content of the SiGe dots [8]. In addition, AFM measurements

indicated that the height and diameter of QDs were 2.96 ± 0.34 nm and 34.21 ± 2.98 nm, respectively. Those dots were then covered by a 100-nm-thick Si cap layer. The details of fabrication and characterization of the studied QD crystal has been reported elsewhere [2, 7].

III. NUMERICAL METHOD

Arrangement of these QDs composed a nanoscaled cubic crystal with lattice constants of 11 nm (denoted by L), 90 nm, and 100 nm. The corresponding lattice dynamics was explored based on the 3D FDTD method with parallel computing in a PC cluster system [9]. Here, the longitudinal acoustic phonons with wavevectors along the surface normal z, i.e., one of the principal axes of the studied lattice, were specially addressed for comparing with the experiment [7]. It was noticed that the lattice constant along the concerned propagation direction was much longer than the other two (11 nm $\ll$ 90 nm and 100 nm). We thus divided the unit cell of the nanocrystal by anisotropic grids ($\Delta x : \Delta y : \Delta z = 10 : 10 : 1$) in the numerical modeling.

One remarkable feature for our low-aspect-ratio unit cell is that the frequencies of forbidden bands along the z axis are much higher than the frequencies of the eigenmodes traveling on the x-y plane. As result, for longitudinal acoustic waves propagating along the z axis with a band-gap frequency, several eigenmodes (high-order mode patterns on the x-y plane) are expected to exist due to long lateral characteristic lengths. This feature is analogous to the light propagation in a multimode fiber and makes the assignment of the calculated eigenmodes in the studied QD crystal difficult. Without loss of feasibility, we adopted an alternative method to calculate the dispersion curves of low-order longitudinal modes, which has been observed experimentally.

In the numerical model, a Gaussian-like strain pulse with a 400-fs duration and a planar wavefront was incident into the QD crystal. We then recorded temporal and spatial evolutions of the laterally-averaged displacements in the QD crystal. By performing 2D (z-t) Fourier transform, the dispersion curves of the longitudinal modes along the z axis can be obtained. It should be mentioned that the displacement field was laterally averaged, which suppressed the detected signals of high-order modes and thus made the concerned fundamental mode clear. The material parameters used in our calculation were taken from Ref. 10.

IV. RESULTS AND DISCUSSIONS

Fig. 2(a) shows the square of the laterally-averaged displacement in the QD crystal under the excitation of an impulsive longitudinal stress T_{zz}, exhibiting two folded dispersion curves. To look into the nature of the split longitudinal modes in details, we numerically investigate the displacement fields at $k_z = 1.5\,\pi/L$, where two braches start to split in the dispersion curves. Figs. 2(b) and 2(c) show the calculated 3D displacement fields in one

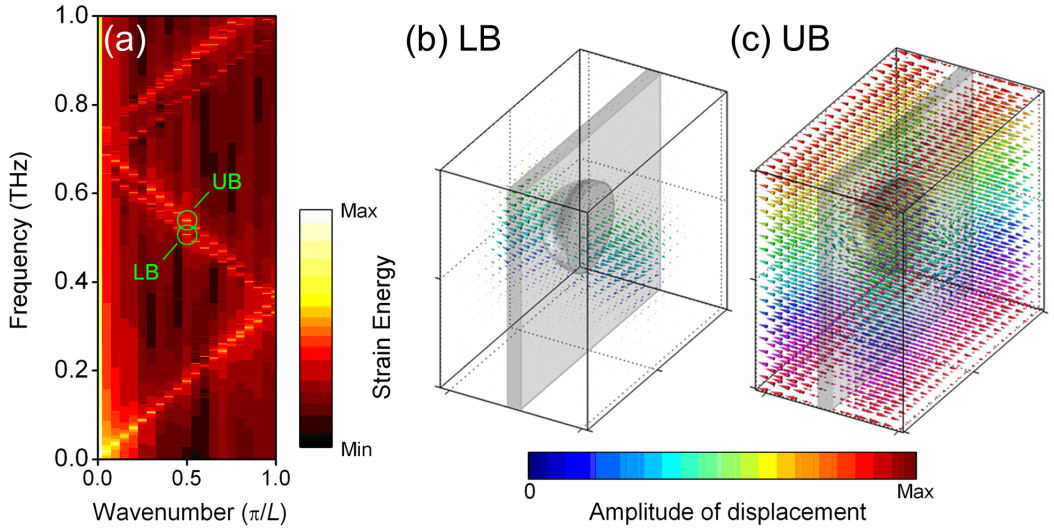

FIG. 2: (a) The band structure image by combining FFT power spectra of square of the laterally-averaged displacements in the QD crystal under an impulsive excitation, indicating the dispersion relations of low-order longitudinal acoustic phonons traveling along the surface normal z. Upper and lower branches (UB and LB) are denoted at $k_z = 1.5\ \pi/L$. (b) and (c) are the corresponding 3D displacement fields in the unit cell. The wetting layer and the QD are shown in gray. Those two figures are extended in the growth direction by five times in order to illustrate the detailed displacement fields.

unit cell for the two different branches. For the lower branch (507.2 GHz), the displacement field can be found to be mainly localized in regions between vertically aligned QDs, i.e., the region corresponding to the QD. For the upper branch (538.8 GHz), the whole unit cell moves, and the phases of the lattice motion in and out of the QD regions are opposite.

Quantization of the propagation modes is a consequence of the lateral Bloch condition (x and y axes) of the 3D crystal, similar to the discrete propagation modes in optical/acoustic waveguides (2D confinement). The higher-order propagation modes traveling in the z direction also exist in the studied system; however, they are not observed in this calculation due to the uniform plane-wave excitation and the data averaging. From Fig. 2(a), it is also found that the QD-induced phonon scattering results in two mini-gaps (0.34 and 0.7 THz) in the sub-THz range. In the following calculations, we focus on the phonon reflection and tunneling at frequencies within the band gaps.

For the calculation of the acoustic reflection and transmission spectra, we considered 10 QD layers (QD crystal) placed in between Si substrate and Si cap layer. Absorbing boundary conditions were made to avoid acoustic reflection from the boundaries of the Si substrate and the cap layer. Here, we recorded the laterally-averaged displacements at positions above and below the QD crystal by 20 nm as a function of time delay, after the excitation of impulsive plane waves (400-fs duration). The amplitude reflection R and transmission T spectra of the QD crystal can then be estimated by comparing the

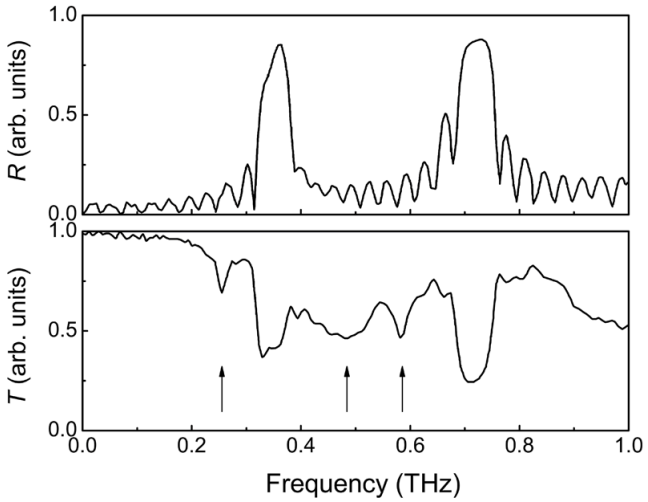

FIG. 3: Calculated amplitude reflection R (top) and transmission T (bottom) spectra of the QD crystal. The arrows denote the transmission reduction (250, 480, and 580 GHz) in addition to the effect of phononic band gaps.

spectra of the incident, reflected, and transmitted waves, as shown in Fig. 3. Significant acoustic reflection at $\sim$0.34 and 0.7 THz was observed, revealing the forbiddance of acoustic propagation at the band-gap frequencies. In addition to the feature of the forbidden bands, periodic side peaks in the reflectivity spectrum were induced by the finite number of the vertical periods. (For finite-period phononic crystals, multiple internal reflections at the crystal boundaries induce oscillatory acoustic reflectivity in the frequency domain, analogous to the Fabry-Perot effect in optics [5].) In addition, the limited number of QD period makes the tunneling of acoustic phonons possible, resulting in non-zero transmission coefficient at the band-gap frequencies. Except the feature of the forbidden bands, we can find additional reductions in transmission coefficient at several specific frequencies, as denoted by the arrows in Fig. 3. These transmission reductions reveal scattering loss of the longitudinal acoustic waves as one compares the transmission and reflection spectra.

Because acoustic attenuation has not been considered in the presented calculation, the observed transmission reduction indicated the transduction of longitudinal acoustic waves into other propagating or vibration modes. To clarify its origin, we compared the transmission spectrum of the QD crystal and that of a similar structure without the QDs, as shown in Fig. 4. Without considering the QD contributions, the crystal with only the wetting layers becomes a 1D structure. The corresponding spectrum shows transmission reductions only at the band-gap frequencies. This analysis provides clear evidence that the observed energy transduction in the QD crystal is induced by the QD-related acoustic scattering and/or confinement.

One of the possible interpretations is the excitation of the interface wave propagating on the planes of the dot layers. Coupling between bulk waves and interface waves typically

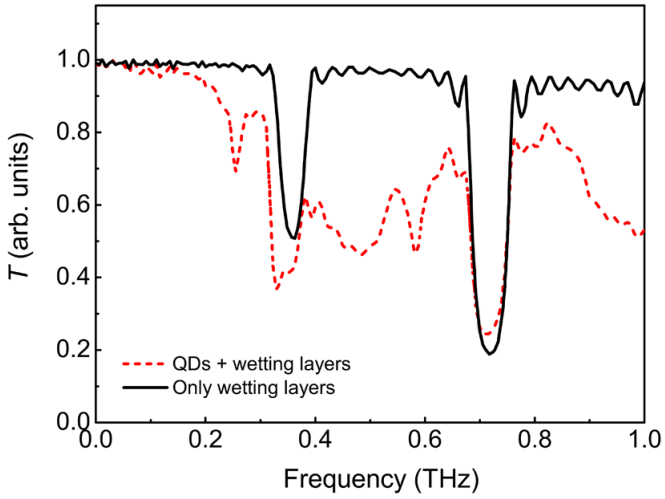

FIG. 4: Calculated amplitude transmission T spectra of the QD crystal, including QDs and wetting layers, and a similar structure without considering the QDs, i.e., only wetting layers.

occurs when the bulk waves is scattered at a corrugated interface, and vice versa. In the concerned structure, the QDs could serve as the responsible scatters transducing the energy. However, the resonant frequency of the interface waves due to the lateral periodicity was calculated to be on the order of 26 GHz [11]. It is much lower than the observed frequencies of energy transduction (250, 480, and 580 GHz). The obvious difference in the resonant frequencies makes this interpretation questionable, and suggests the possibility of acoustic vibrations in a structure with smaller dimensions, i.e., higher resonant frequencies.

Vibration of isolated QDs has been observed in many material systems, which can be excited by femtosecond lasers [3] or through direct coupling between sub-THz photons and phonons [12]. For typical semiconductor QDs, the frequency of confined acoustic modes is typically in the sub-THz range (0.1–1 THz), supporting that the observed loss of sub-THz longitudinal bulk waves could be due to the coupling with the confined vibrations of isolated QDs.

V. CONCLUSIONS

The phononic band-gap effect of 3D ordered quantum dots was investigated by the FDTD methods. The observed phononic band gaps in the sub-THz regime result in high acoustic reflectivities of the nanocrystal at the band-gap frequencies. In addition to the phononic band gaps, the acoustic transmission spectrum reveals remarkable energy transduction at several specific frequencies. It could suggest the coupling between the longitudinal acoustic phonon and confined modes of isolated quantum dots.

Acknowledgments

The authors would like to acknowledge Jin-Wei Shi for technical support. This work was sponsored by National Science Council of Taiwan under the Grant NSC–98–2120–M–002–001 and the MediaTek Fellowship.

References

* Electronic address: ycwen@phys.sinica.edu.tw

[1] M. Cazayous, *et al.*, Phys. Rev. B **66**, 195320 (2002).
[2] D. Grützmacher, *et al.*, NanoLett. **7**, 3150 (2007).
[3] See, for example, T. D. Krauss and F. W. Wise, Phys. Rev. Lett. **79**, 5102 (1997).
[4] A. Devos, *et al.*, Phys. Rev. Lett. **98**, 207402 (2007).
[5] N. D. Lanzillotti-Kimura, *et al.*, Phys. Rev. B **75**, 024301 (2007).
[6] See, for example, P. D. Lacharmoise, *et al.*, Phys. Rev. B **76**, 155311 (2007), and references therein.
[7] Y.-C. Wen, *et al.*, Appl. Phys. Lett. **96**, 123113 (2010).
[8] V. Holy, *et al.*, Phys. Rev. B **79**, 035324 (2009).
[9] P.-F. Hsieh, *et al.*, IEEE Trans. Ultrason., Ferroelect., Freq. Contr. **53**, 148 (2006).
[10] D. J. Lockwood, *et al.*, Phys. Rev. B **35**, 2243 (1987).
[11] The velocity of Rayleigh wave on the Si surface is 4680 m/s. With a lateral period of 90 nm, the fundamental resonant frequency of the Rayleigh waves can be calculated to be $\sim$26 GHz, which should be on the same order of the characteristic frequency of the interface-wave resonances between the QDs.
[12] T.-M. Liu, *et al.*, Appl. Phys. Lett. **92**, 093122 (2008).